



Enhancing the Surface Quality and Tribomechanical Properties of AA 6061-T6 Friction Stir Welded Joints Reinforced with Varying SiC Contents

Taiwo Ebenezer Abioye, Hussain Zuhailawati , Abu Seman Anasyida, Sulaiman Abimbola Yahaya, and Muhammad Nabil Faizul Hilmy

Submitted: 22 January 2020 / Revised: 17 February 2021 / Accepted: 19 March 2021 / Published online: 26 April 2021

Obtaining high-quality AA6061-T6 weldment is difficult because of the dissolution of its strengthening precipitates at temperatures beyond 250°C. In this work, the surface quality, mechanical and wear properties of AA6061-T6 friction stir welded joints at varying SiC addition (0.56-1.72 g) and number of weld passes (1-6) were investigated and discussed. SiC content was varied by changing the center groove width (CGW). Also, microstructure analysis of the entire welded joints was performed. For the first time, a process map predicting the surface characteristics of SiC reinforced AA6061-T6 friction stir welded joint at varying combinations of CGW and number of weld passes was developed. Increasing the number of passes resulted in better matrix refinement, particles fragmentation and improved particles distribution while increase in SiC content produced particles clustering and lower particles fragmentation. All the reinforced joints showed higher hardness but lower ductility than the unreinforced joint. Only joints reinforced with 0.56 g SiC showed improved tensile strength than the unreinforced joint (156 MPa) with the highest value of ~196 MPa (67% of the base metal) obtained at 4 weld passes. Increased hardness and tensile strength obtained as the weld passes increased from 2 to 4 was traced to better grain refinement, improved particles distribution and fragmentation. However, slight reduction in these properties at 6 passes was observed. Ductile fracture mode was found in all the joints except for joints reinforced with 1.01-1.72 g of SiC that showed evidence of brittle fracture. The specific wear rates of the entire reinforced joints are lower than that of the unreinforced joint. The weldment formed with 0.56 g SiC addition at 4 weld passes exhibited the best combination of properties among the entire weldments.

Keywords aluminum alloy 6061-T6, friction stir welding, mechanical properties, SiC reinforcement, weld passes, wear resistance

1. Introduction

A precipitation hardened AA 6061 (i.e., AA 6061-T6) is now widely being applied for manufacturing wheel rims, engine chases and car frames in automotive industry, wings and fuselages in aerospace industry and some structural components in the marine and railway industries (Ref 1, 2). These are due to some unique properties of this aluminum alloy such as high strength to weight ratio, excellent corrosion resistance, high toughness, good ductility and low cost (Ref 3). In the

process of fabricating large-sized aluminum components, friction stir welding is currently the most suitable joining method because the joint quality is not limited by the high thermal conductivity, high reflectivity (Ref 4) and surface oxide layer formation (Ref 5) that characterise aluminum alloys. However, the dissolution of the strengthening precipitate (β'' -Mg₅Si₆) at the welded joint is an issue of concern peculiar to welding of AA 6061-T6 (Ref 6). As a result, mechanical and wear resistance properties at the joint are inferior compared to the other parts of the weldment. In order to overcome this challenge, several efforts including optimisation of the process parameters (Ref 7), post-heat treatment of the weldment (Ref 8) and addition of reinforcement particles at the joint to form metal matrix composites (MMCs) (Ref 9) have been tried.

Among these, addition of reinforcement is increasingly receiving attention because of the availability of the reinforcement particles. Several reinforcement particles including ceramics (SiC, Al₂O₃, WC, B₄C) (Ref 10, 11), agricultural waste products (rice husk, cow horn, fly ash) (Ref 12, 13), carbonaceous particles (graphite, carbon nanotubes and graphene) (Ref 14) and metal chips (Cu, stainless steels) (Ref 15, 16) have been tried and yielded obvious improvement in the joint quality. For example, *Khojastehnezhad and Pourasl* (Ref 17) investigated the microstructure and mechanical properties of AA 6061-T6 reinforced with and without Cu plate insert. Defect-free weldments were obtained at a rotational speed of 950 rpm and traverse speed of 50 mm min⁻¹. Weldments with the Cu plate insert showed higher hardness and tensile strength due to higher dislocation density and strong metallurgical bonding between the Al matrix and Cu insert. Effects of SiC

Taiwo Ebenezer Abioye, Structural Materials Niche Area, School of Materials and Mineral Resources Engineering, Engineering Campus, Universiti Sains Malaysia, 14300 Nibong Tebal, Penang, Malaysia; and Industrial and Production Engineering Department, School of Engineering and Engineering Technology, Federal University of Technology Akure, PMB 704, Akure, Ondo State, Nigeria; **Hussain Zuhailawati**, **Abu Seman Anasyida**, and **Muhammad Nabil Faizul Hilmy**, Structural Materials Niche Area, School of Materials and Mineral Resources Engineering, Engineering Campus, Universiti Sains Malaysia, 14300 Nibong Tebal, Penang, Malaysia; **Sulaiman Abimbola Yahaya**, School of Mechanical Engineering, Engineering Campus, Universiti Sains Malaysia, 14300 Nibong Tebal, Penang, Malaysia. Contact e-mail: zuhaila@usm.my.

addition on the microstructure and mechanical properties of the friction stir processed AA 6061-T4, using double tool passes, have been investigated by *Choi et al.* (Ref 18). Better grain refinement was achieved with the SiC addition producing harder surface (75 HV) than the surface without reinforcement (55 HV).

It has been established that the quality of the metal matrix composite joints is influenced by some factors such as type, size, shape and volume of reinforcement particles in the matrix (Ref 19). Other factors include particles distribution homogeneity, degree of aluminum matrix grain refinement and particles fragmentation which can be controlled by the number of weld passes. Compared with SiC and Al₂O₃, B₄C reinforced AA 6061-T6 friction stir welded joint has been found to have highest hardness, while SiC addition showed the lowest wear rate (Ref 20). Likewise, Sahraeinejad et al. (Ref 21) investigated the mechanical properties of the AA 5059 surface that was reinforced with SiC, Al₂O₃, B₄C particles using friction stir processing technique. B₄C reinforced surface showed the highest hardness because of the inherent high hardness of B₄C. Nanoparticle's additions have been established to yield better mechanical and wear resistance properties than the micro-particles additions in the MMC joints (Ref 22, 23). Increasing the number of friction stir processing passes has been reported to increase the mechanical and corrosion properties of Zircon reinforced AA 5052 composite (Ref 24). So far, single and double weld passes are usually applied during FSW of AA 6061-T6 so as to control the extent of the softening effect (i.e., dissolution of strengthening precipitates) at the joint.

Till date, the mechanical and wear performances of the AA 6061-T6 and other heat-treated aluminum alloy have not been investigated under different weld passes (2-6) and reinforcement contents. The reinforcement content can be changed by varying the width of the center groove created in the workpiece. Though the center groove width has been established to be critical to producing high-quality friction stir welded joint (reinforced) (Ref 25), the surface characteristics of the joints under different weld passes and center groove widths have also not been analyzed in the past. In this work, FSW of SiC reinforced AA 6061-T6 was carried out at optimised process parameters. The surface quality, microstructure, mechanical and tribological properties of welded joints were investigated at varying reinforcement contents and weld passes. A process map predicting the visual surface characteristics of the SiC reinforced AA 6061-T6 joints at varying SiC contents and weld passes was developed.

2. Materials and Methods

2.1 Materials Preparation and Welding Process

As-received AA 6061-T6 rolled sheet (i.e., base metal) was machined to 18 plates, each of dimension 100 × 50 × 6 mm (L × B × H). The chemical composition (wt.%) of the AA 6061-T6 is Al, 98.08; Mg, 0.51; Si, 0.63; Zn, 0.06; Cr, 0.06; Mn, 0.02; Fe, 0.30; Ni, 0.02; Cu, 0.31; Ga, 0.01. The plates were temporarily joined together in pairs and machined at the center so as to produce nine samples with different center groove profiles, as detailed in Table 2. Thereafter, the grooves were filled with SiC particles (average size of 6 μm) and later

closed by passing a rotating pinless friction stir tool over them. This was done so as to prevent sputtering of the SiC particles during friction stir welding (FSW) process. The average mass (g) and volume of the SiC powder contained in each groove are given in Table 1. Figure 1 presents the scanning electron micrographs and XRD spectrum of the SiC utilised in this work.

Each sample was friction stir welded producing a total of nine weldments. A tapered pin tool made with high speed steel was used. The tool shoulder is of diameter 20 mm while the tool pin is of length 4.5 mm and diameter 4 mm at the tip. Based on the findings from the previous work of the authors Ref 26, the entire welding process was performed at tool rotational speed of 850 rpm, traverse speed of 45 mm min⁻¹ and tilt angle of 2.5°. The welding was performed along the center groove with about 1 mm offset to the retreating side (RS) so as to improve material flow to the RS. As detailed in Table 1, the number of FSW passes utilised ranged from 2 to 6 for each average mass of SiC added with a minimum time-gap of ~7 min in between two successive passes. All welding passes were along the same direction in order to enhance even distribution of the reinforcement particles. Following similar procedures, FSW of AA 606-T6 without reinforcement was also performed so as to serve as a reference.

2.2 Microstructure Analysis

Samples of dimension 20 × 10 × 6 mm were transversely cut from the friction stir welded joints (FSWJs). The cross-sectioned surfaces were cleaned, ground and polished to 0.3 μm surface finish. The surfaces were later etched using modified Poulton's reagent (50 ml Poulton's reagent + 25 ml HNO₃ + 1 ml HF + 1 ml H₂O) for about 5-7 s. Thereafter, the grain structure and grain size of the samples (i.e., welded joints) were examined using Xoptron optical microscope (X-80 series) equipped with digital microscope image analyzer. The reinforcement particles distribution and Si composition (wt.%) in each joint after FSW were determined using a combination of scanning electron microscopy (SEM) and energy-dispersive x-ray spectroscopy (EDX). The difference between the Si composition in each joint and in the as-received aluminum alloy (i.e., base metal) was used to estimate the amount of SiC retained in the joint after the FSW. The SiC size in each FSW joint was determined using an image J processing software and analyzing at least three SEM images taken at the top, middle and bottom regions of the stir zone.

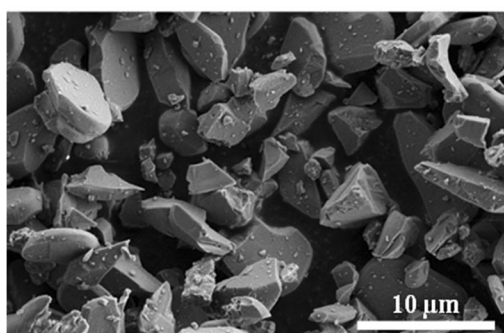
2.3 Mechanical and Wear Tests

Vickers micro-hardness measurements of the FSWJs and the base metal were performed along and across the cross-sectioned surface of the joints by using 300 gF load for a dwell time of 10 s. A minimum spacing of about 1.5 mm was allowed in between two successive indentations so as to improve the reliability of the results obtained. Tensile tests were done using Instron universal testing machine at a constant cross-head of 0.5 mm min⁻¹. Three tensile specimens (cut across the joint) were prepared from each weldment following ASTM E8/E8M-13. The average of the results obtained from the three specimens represents the tensile properties of the weldment. The base metal specimens were also prepared and tested following similar standard.

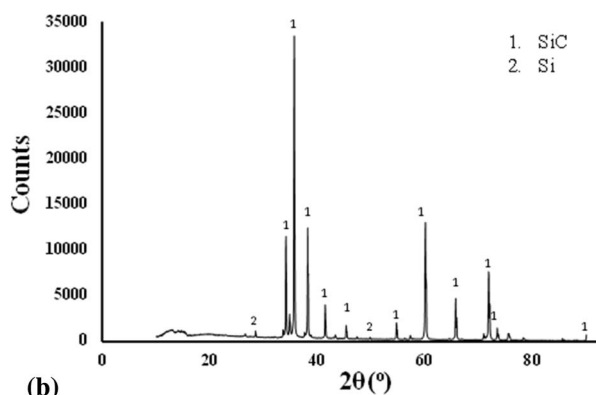
Wear tests were performed on the friction stir welded and base metal surfaces using pin-on-disk methods. The tests were

Table 1 Processing conditions for the friction stir welding

Samples	Groove size, mm	Mean mass of SiC added, g	Mean volume of SiC added, mm ³	Number of weld passes
A1	95 × 1.5 × 4.5 (L × W × H)	0.56	176	2
A2				4
A3				6
B1	95 × 2.5 × 4.5	1.01	312	2
B2				4
B3				6
C1	95 × 3.5 × 4.5	1.72	535	2
C2				4
C3				6



(a)



(b)

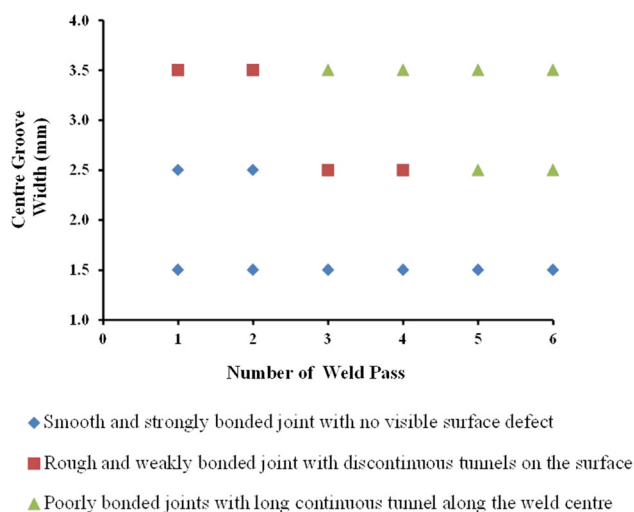
Fig. 1 (a) SEM image showing SiC particles size and shape, (b) XRD spectrum of the as-received SiC particles

performed at room temperature using 20 N and 50 N loads, varying sliding distance (200-1000 m), sliding speed of 0.3 m s⁻¹ and disk speed of 48 rpm. The utilised disk (Ø = 120 mm) is made of hardened EN-31 carbon steel of hardness 62 HRC. The weight in gram of the sample before and after each test run was measured and recorded. The volume loss in mm³ (V_L) was calculated by $V_L = (W_L \times 1000)/\rho$ where W_L is the weight loss in g and ρ is the density of each sample in g.cm⁻³. The specific wear rate (SWR) in mm³ N⁻¹ m⁻¹ of each sample was determined using $SWR = V_L/(S_d \times L)$ where L is the applied load in N and S_d is the sliding distance in m. The friction coefficient was recorded automatically by the wear testing machine. The worn surfaces of the samples were analyzed using SEM.

3. Results and Discussion

3.1 Visual Surface Characteristics of the Weld Joints

Visual observation of the FSWJs revealed that their bonding strength and surface quality varied as the center groove width (CGW) and number of weld passes changed. The weld joints produced at varying CGWs (1.5-3.5 mm) with increasing number of weld passes (1-6) were classified into three, as presented in the process map shown in Fig. 2. The three joints visual characteristics, as shown in Fig. 3, are (i) smooth and strongly bonded joint with no visible surface defect, (ii) rough and weakly bonded joint characterised with discontinuous tunnels at the surface and (iii) poorly bonded joint characterised with continuous tunnels at the surface. The process map

**Fig. 2** A process map showing SiC-reinforced AA 6061-T6 friction stir welded joints visual characteristics at different center groove width with increasing weld passes. (Rotation speed of 850 rpm, traverse speed of 45 mm min⁻¹, tool tilt angle of 2.5°C, tapered tool pin diameter of 4 mm at the tip)

presented in Fig. 2 is valid for SiC reinforced AA 6061-T6 FSWJ under optimal parameter settings of 850 rpm rotational speed, 45 mm min⁻¹ traverse speed and 2.5° tilt angle. The tool pin is tapered with 4 mm diameter at the tip. Figure 3 presents the typical examples of FSWJs produced for each CGW as the number of weld passes increased. As shown in Fig. 3a, smooth and strongly bonded FSWJs with no visible surface defects

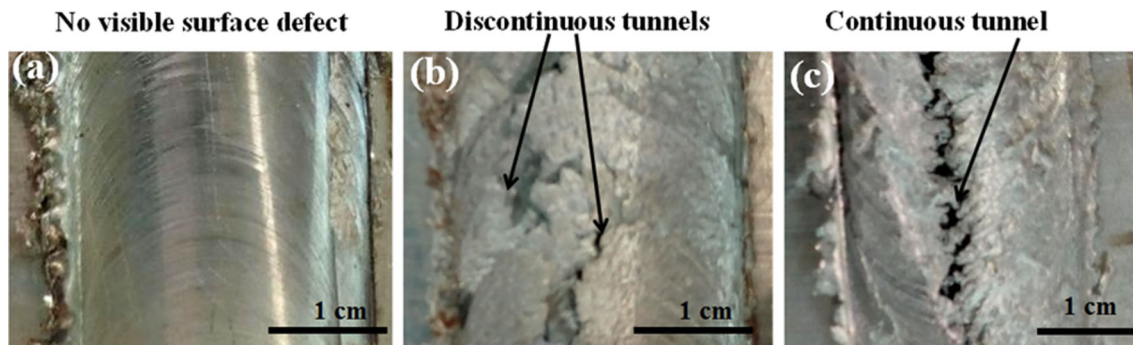


Fig. 3 Typical examples of the visual characteristics of the SiC-reinforced AA 6061-T6 friction stir welded joints (a) smooth and strongly bonded joint with no visible surface defect, (b) rough and weakly bonded joint characterised with discontinuous tunnels at the surface and (c) poorly bonded joint characterised with long continuous tunnels along the weld center

were produced when the CGW was 1.5 mm for the number of weld passes ranging from 1 to 6. This joint characteristic is considered ideal for the FSW of SiC reinforced AA 6061-T6 because no visible defects were found on the surface and strong bonding is observed at the joint. This was found possible because the CGW was relatively small and the volume of reinforcement is also small. Therefore, sufficient volume of aluminum alloy (i.e., matrix) was plasticised hence, the material flow was efficient. Also, the volume of reinforcement added was not sufficient enough to hinder the stirring and flow of plasticised aluminum alloy. As a result, defect-free and strongly bonded joints with smooth surface were produced with 1.5 mm CGW. Similar observation was found by Bodaghi and Dehgani (Ref 27) when the CGW was set below 2 mm during FSW of AA 5052 with SiC nanoparticles addition. The surface smoothness was observed to improve as the number of weld passes increased because the process temperature increased with increasing the weld passes (Ref 28). This invariably increased the matrix material plasticity hence, enhanced matrix material flowability which resulted in drawing of more aluminum alloy to the stir zone.

At 2.5 mm CGW, ideal joint characteristic was obtained with single and double weld passes only. Rough and weakly bonded FSWJs characterised with discontinuous tunnels at the surface were obtained with 3 and 4 weld passes, while poorly bonded FSWJs characterised with continuous tunnels along the weld center were found when the number of weld passes was 5 and 6. Generally, increasing the CGW while keeping other conditions fixed implies that the volume of reinforcement added increased, whereas the matrix (i.e., the aluminum alloy) volume reduced in the stir zone. This is believed to have hindered the stirring action and matrix material flowability during FSW process. Ideal joint characteristics obtained with 1 and 2 weld passes suggest that the sufficient matrix alloy flowed into SZ and stirring of this volume of material was sufficient to give proper bonding. Hence, no visible defects were observed. At 3 weld passes and beyond, the process temperature increased but continuous drawing of matrix alloy into the SZ was difficult due to large CGW. As a result, re-stirring of the materials already contained in SZ (which has high content of reinforcement particles) largely occurred. Due to this, defects such as tunnel and poor surface quality were initiated.

At 3.5 CGW, the amount of matrix alloy that was being stirred was insufficient. Therefore, stirring of reinforcement particles largely occurred and proper bonding did not occur.

Therefore, no joint with ideal characteristic was produced, at 3.5 CGW, for all the number of weld passes (1-6) utilised in this work. Finally, it can be inferred from this process map that smooth and strongly bonded SiC particles reinforced AA 6061-T6 FSWJs with no visible surface defect can be obtained when the CGW is 1.5 mm for 1 to 6 passes. This can also be achieved for up to double passes when the center groove width is 2.5 mm. Outside this condition, it is practically difficult to obtain smooth reinforced FSWJ without any visible surface defect.

3.2 Microstructure Analysis

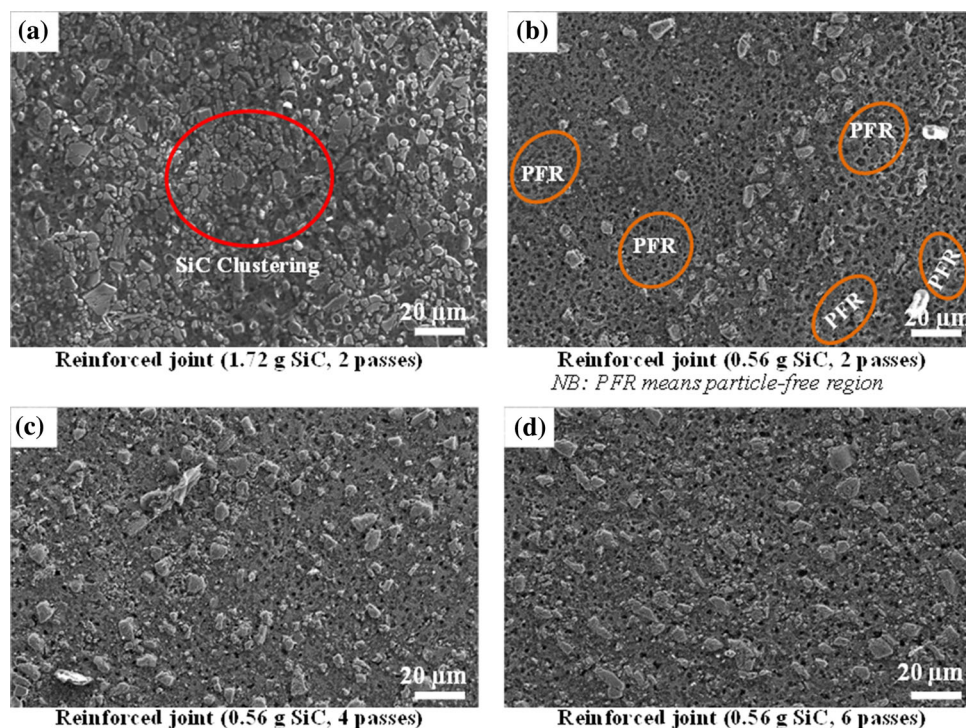
Microstructure analysis was carried on some samples cut from the surface defect-free joints. Samples A1, A2 and A3 were obtained from the defect-free joints produced with 1.5 mm CGW at 2, 4 and 6 weld passes, respectively. As previously presented in Table 2, the mass of SiC added in these joints is average of 0.56 g. In order to investigate the effect of varying SiC contents, samples B1, B2 and B3 were also cut from the middle of the joints formed with 1.5 mm, 2.5 mm and 3.5 mm CGW, respectively. The number of weld pass was fixed at 2. Though sample C1 (3.5 mm groove width) was not defect-free (base on visual observation of the weld surface), it was added so as to show trend during the investigation. The mass of the reinforcement in the samples A1, B1 and C1 is average of 0.56 g, 1.01 g and 1.72 g, respectively.

Figure 4 shows the secondary electron (SE) mode scanning electron micrographs of the core of the stir zone of the samples. Though it was previously established that more reinforcement particles are pushed out of the groove as the CGW becomes wider during FSW (Ref 25), the results obtained in this current work reveals that more particles were retained in the FSWJ as the CGW increased. This is partly due to increased volume of SiC added at wider CGW. Also, the sealing of the groove after particles addition by passing pinless tool over the groove also prevented excessive sputtering of the particles during the FSW.

This observation was further established by conducting EDX area scan (200 × 200 μm) analysis randomly at three different regions within the SZ. The average of the results of the EDX analysis for each sample is presented in Table 2. The amount of the retained SiC particles in each sample was estimated by determining the average composition of Si (wt.%) in the SZ. The composition of Si in the as-received AA 6061-T6 has been previously given as 0.63 wt.% (see Table 1). Any increase in the Si composition is evidence of retained SiC particles in the welded joint. Carbon was not quantified because

Table 2 Elemental composition (wt.%) of the stir zones of the reinforced friction stir welded joints

Samples	SiC content, g	No of passes	Mg, wt.%	Al, wt.%	Si, wt.%
C1	1.72	2	0.73 ± 0.1	51.77 ± 2.6	47.50 ± 2.6
B1	1.01	2	1.40 ± 0.1	65.85 ± 1.4	32.75 ± 1.5
A1	0.56	2	1.60 ± 0.3	89.03 ± 0.3	9.36 ± 0.3
A2	0.56	4	1.48 ± 0.1	92.38 ± 0.8	6.13 ± 0.8
A3	0.56	6	1.70 ± 0.2	90.27 ± 1.1	8.03 ± 0.5

**Fig. 4** SEM (SE mode) images showing the SiC particle distribution and extent of fragmentation in the stir zones of some selected reinforced joints

of the limitation of the SEM/EDX technique to accurately quantify it. As seen in Table 2, sample C1 (3.5 mm CGW with ~ 1.72 g SiC added) has an average of 47.5 ± 2.6 wt.% composition of Si, while sample B1 (2.5 mm CGW with ~ 1.01 g SiC added) has an average of 32.8 ± 1.5 wt.%. Sample A1 with 0.56 g added SiC (1.5 mm CGW) has an average of 9.4 ± 0.3 wt.% Si composition in the SZ. This result confirms the fact that the amount of retained SiC in the FSWJ increased as the CGW increased (due to increased SiC particles initially added) during FSW increased.

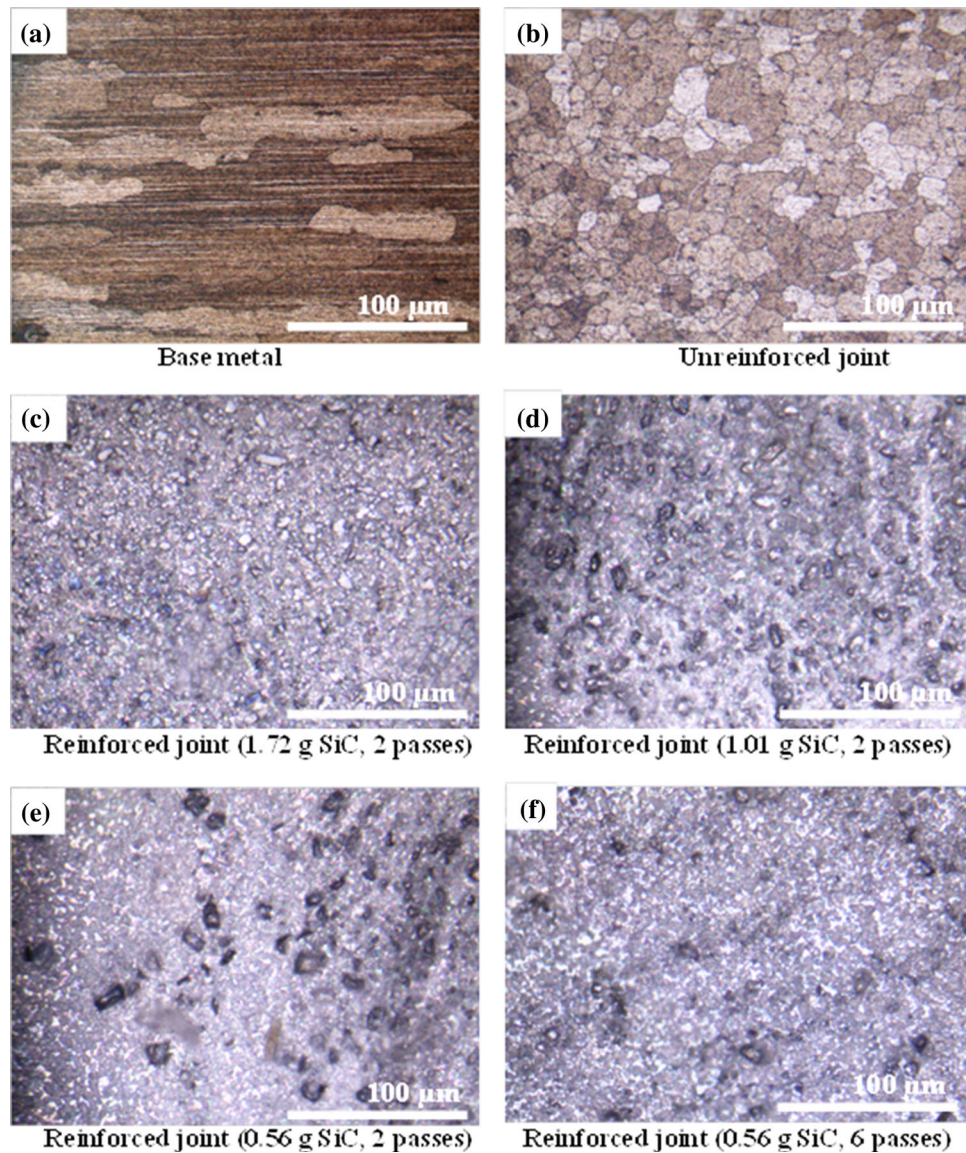
On the other hand, increasing the number of weld passes (in samples A1-A3) was observed to result in more homogenous SiC particles distribution and higher volume of smaller particles. The higher number of particles found in joints formed at higher number of weld passes, as clearly observed in Fig. 4b-d, is due to fragmentation of the added SiC particles into smaller sizes during FSW. The average size of the SiC particles retained in each joints was measured, and the results are presented in Table 3. The average particles size decreased (5.5-4.3 μm) with decrease in the mass of SiC added (1.72-0.56 g). The reason for this is that tool stirring was increasingly being hindered as the amount of reinforcement in the joint increased. Hence, lower degree of fragmentation occurred. Fragmentation

phenomenon caused the breaking of bigger SiC particles into smaller sizes. More significantly, the particles size decreased (4.3-2.2 μg) with increasing the number of weld passes. This is evidence that higher SiC particles fragmentation occurred as the weld passes increased from 2 to 6 (Ref 29).

Optical micrographs revealing the grain structure of the base metal and the stir zones of the unreinforced and some selected reinforced FSWJs are presented in Fig. 5. As presented in Table 3, substantial grain refinement occurred during the friction stir welding because the average grain size in the SZ of the unreinforced joint (~ 19 μm) was significantly lower than that in the base metal (~ 143 μm). This was due to severe plastic deformation causing dynamic recrystallisation in the SZ (Ref 24). Much smaller grain sizes found in the reinforced joints revealed that further aluminum matrix refinement occurred with the SiC addition. This was as a result of pinning effect hindering grain growth, therefore, aiding nucleation of new grains (Ref 19). As seen in Fig. 5c, e, respectively, clustering or agglomeration of the particles was evident in sample C1 (1.72 g SiC, 2 passes) and large particle-free regions were observed in sample A1 (0.56 g SiC, 2 passes).

Table 3 Average sizes of the retained SiC and grains in the joint and base metal

Samples	SiC content, g	No of passes	Average SiC particle size, μm	Average grain size, μm
C1	1.72	2	5.5 ± 0.5	3.6 ± 0.8
B1	1.01	2	4.8 ± 0.5	5.1 ± 1.1
A1	0.56	2	4.3 ± 0.3	8.9 ± 1.6
A2	0.56	4	3.7 ± 0.4	7.8 ± 1.3
A3	0.56	6	2.2 ± 0.3	6.3 ± 1.5
Unreinforced joint	...	2	...	19.1 ± 1.4
Base metal	143.3 ± 11.3

**Fig. 5** Optical micrographs of the (a) base metal and SZs of the (b) unreinforced and (c-f) some selected SiC-reinforced AA 6060-T6 friction stir welded joints

3.3 Micro-Hardness

Figure 6 presents the hardness profile of the reinforced AA 6061-T6 joints at varying SiC contents and different number of FSW passes. As revealed in Fig. 7a, b, the SZ of the entire FWSed-joints exhibited higher hardness than the thermo-mechanical affected zone (TMAZ). This is attributed to higher

concentration of the reinforcement particles in the SZ as compared with the TMAZ. Also, increased plastic deformation in the SZ is believed to have caused higher particles fragmentation. Therefore, dynamic recrystallisation and pinning effect (due to higher particles concentration) phenomena causing enhanced grain refinement are more prominent in the

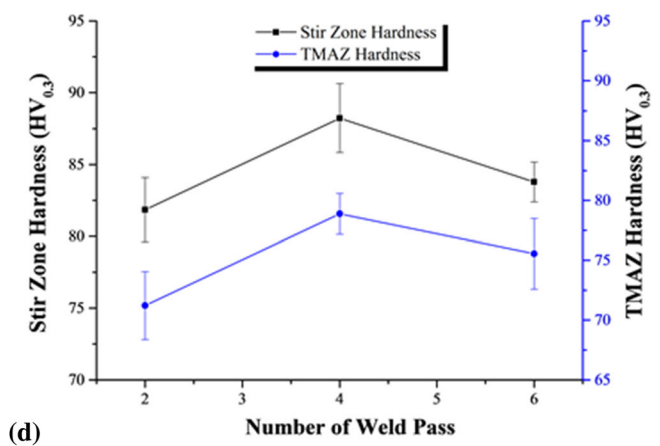
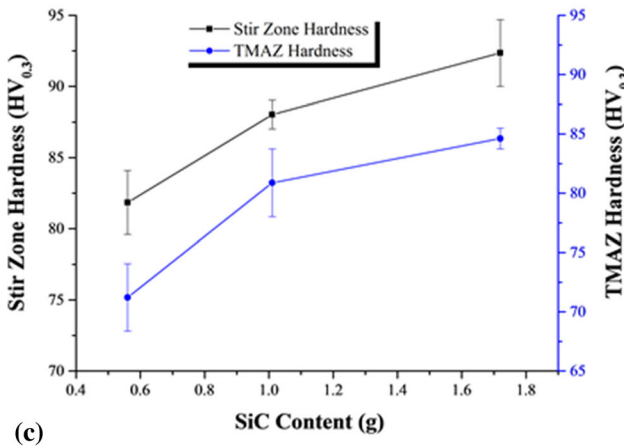
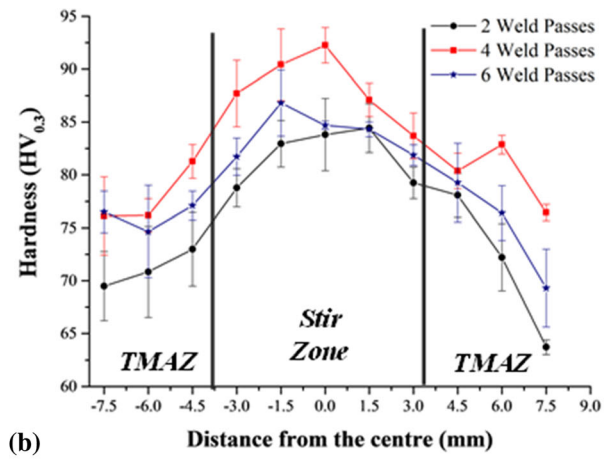
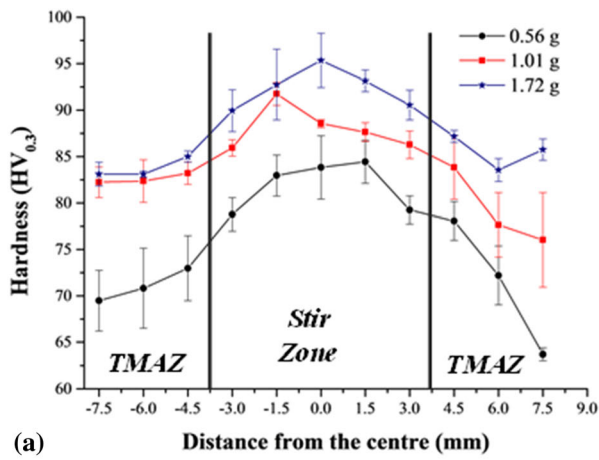


Fig. 6 Hardness profiles of the SiC reinforced AA 6061-T6 at varying reinforcement contents and different weld passes

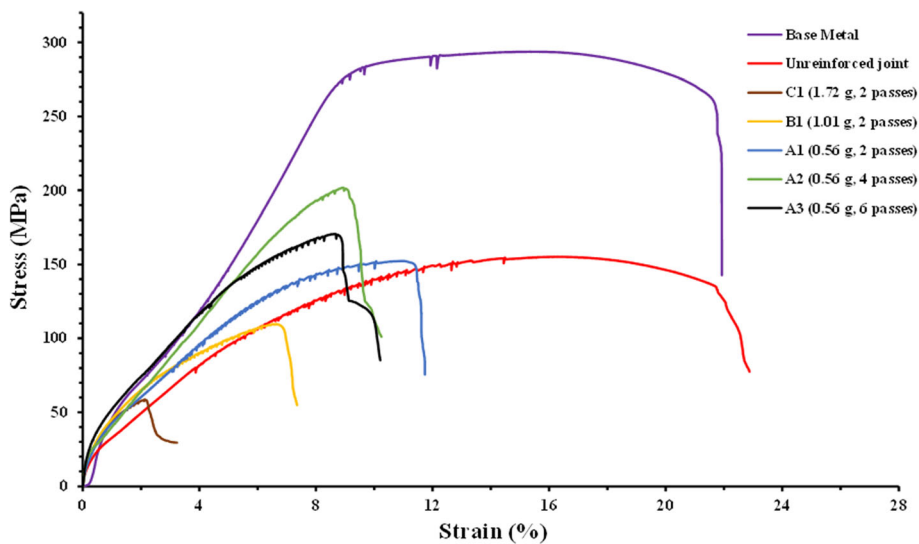


Fig. 7 Stress vs strain curves of the base metal and the friction stir welded joints

SZ [6, 19]. Consequently, the hardness is higher in the SZ. Also, the hardness of the reinforced welded joints (SZ & TMAZ) increased with increasing the SiC content. As the SiC content increased from 0.56 g to 1.72 g, the SZ and TMAZ

hardness increased from 81.9 to 92.4 HV_{0.3} (12.8% increase) and 71.2 to 84.6 HV_{0.3} (18.8% increase), respectively.

Increasing the number of weld passes from 2 to 4 (at 0.56 g SiC content) resulted in about 7.7% rise in SZ hardness (81.9-88.2 HV_{0.3}), as presented in r. 7d. At 6 weld passes, the

hardness declined by 4.4% from 88.2 to 83.8 HV_{0.3}. The hardness of the TMAZ follows similar trend as the number of weld passes increased from 2 to 6. The hardness of the unreinforced FSWJ and the as-received AA 6061-T6 (base metal) was found to be average of 65 ± 3.4 HV_{0.3} and 113 ± 2.3 HV_{0.3}, respectively. This indicates that all the reinforced FSWJs exhibited higher hardness than the unreinforced joint but are closer to the base metal depending on the SiC content and number of weld passes.

The significant reduction in the hardness of the unreinforced FSWJ compared with the as-received metal has been previously discovered to be due to the dissolution of strengthening precipitates (β'' -Mg₂Si₆) in the microstructure of the AA 6061-T6 (age hardened AA 6061) [6]. Improved hardness demonstrated by all the reinforced joints is the direct result of the SiC particle reinforcement. By increasing the number of weld passes at fixed SiC addition, the increase observed from 2 to 4 passes is due to (i) enhanced fragmentation of the SiC particles and (ii) better distribution of the particles as a result of increased stirring. These two factors are adjudged to have caused enhanced grain refinement due to higher degree of dynamic recrystallisation and pinning effect [30]. Though further heat generation due to increased number of passes (2-4) is believed to have caused further dissolution of the strengthening precipitates, the increased hardness observed is a proof that the positive effects of the increased fragmentation and improved homogeneous particles distribution are more significant. However, the slight decline in hardness as the number of passes increased from 4 to 6 could be attributed to the fact that more heat was generated leading to further dissolution of the remaining strengthening precipitates. The decline in hardness shows that the softening effect due to the precipitate's dissolution is more significant than the effects of the increased fragmentation and improved homogeneous particles distribution at this welding condition (Ref 1, 6, 31)

3.4 Tensile Properties

Figure 7 presents the stress vs strain curves obtained for the base metal and the friction stir weldments during the tensile test. The summary of the results presented in Fig. 7 is given in Table 4. The as-received metal exhibited the best tensile properties with ultimate tensile strength (UTS) of ~ 290 MPa, yield strength (YS) of ~ 288 MPa and percentage elongation (PE) of ~ 23.6%. The unreinforced weldment exhibited significant reduction in the UTS (~ 156 MPa) and YS (~150 MPa) which are about 46% and 48%, respectively. However, its PE (~21.2%) is very much close to that of the base metal. The decrease in UTS and YS can also be traced to the dissolution of the strengthening precipitates during welding causing loss of structural strengthening in the welded joint. The occurrence of grain refinement in the unreinforced FSWJ showed no signif-

icant impact on the UTS. However, it is believed to have positively influenced the ductility of the weldment since PE of the unreinforced weldment is very close (~90%) to that of the BM.

The results obtained for samples A1, B1 and C1 reveal the effects of increasing SiC content and increasing CGW on the tensile properties of the weldments. Sample C1 with CGW of 3.5 mm and SiC content of 1.72 g demonstrated the least tensile properties (UTS = ~ 60 MPa, YS = ~ 58.3 MPa and PE = ~ 3.5%). This is even much lower than that of the unreinforced weldment. However, as the CGW and SiC addition reduced to 1.5 mm and 0.56 g, respectively, in sample A1, the UTS increased to ~159 MPa, the YS increased to ~152 MPa, while the PE rose to about 9.8%. Even at this condition (0.56 g, 1.5 mm CGW, 2 passes), the PE (i.e., ductility) is still low. The improvements in the UTS and YS were insignificant, as compared with the unreinforced weldment.

Significantly poor tensile properties (strength and ductility) exhibited by the sample C1 are first due to excessively large CGW. The 3.5 mm CGW, as previously explained in Sect. 3.1, produced weak joint with evidence of tunnels on the joint surface. Areas around the tunnel are potential sites for fracture initiation whenever the joint is under tension. Also, the high content of SiC resulted in the clustering of the particles (see Fig. 4). This is adjudged to have resulted in weaker cohesion between the retained SiC and the aluminum matrix because *Jamalian et al.* (Ref 29) have established that particle's agglomeration in composite joints reduces ceramic-matrix cohesion. Finally, the overall fracture toughness of the entire joint is believed to have decreased substantially because of the high ceramics content. Generally, ceramic is known to be extremely hard and brittle with high fracture tendency. Therefore, increasing ceramic content will increase the fracture propensity of a composite joint (Ref 20). Hence, weldment with poor strength and ductility was formed. As the SiC and CGW decreased, better joint characteristic is found and particles clustering reduced. Hence, the UTS and YS were enhanced.

The ~24% increase in the UTS, ~22% upsurge in YS and ~18 % rise in PE demonstrated by the sample A2 (0.56 g, 1.5 mm CGW, 4 passes) over the sample A1 (0.56 g, 1.5 mm CGW, 2 passes) can be traced to improved particles distribution homogeneity, increased particles fragmentation and substantial improvement in aluminum grain refinement. This is in agreement with the finding of *Rahsepar and Jarahimoghadam* (Ref 24) during multi-pass friction stir processing of zircon-reinforced aluminum matrix composites. The increased stirring at 4 weld passes resulted in better particles distribution and higher fragmentation of the SiC into smaller particles. Hence, higher UTS, YS and PE were achieved. The slight decline in the UTS and YS but increase in PE as the number of passes increased to 6 is an indication that the effects of the particles fragmentation

Table 4 Summary of the tensile test results

Samples	Base metal	Unreinforced joint	C1 (1.72 g, 2 passes)	B1 (1.01 g, 2 passes)	A1 (0.56 g, 2 passes)	A2 (0.56 g, 4 passes)	A3 (0.56 g, 6 passes)
Elongation (%)	23.6 ± 0.9	21.2 ± 1.0	3.4 ± 1.6	5.7 ± 2.8	9.8 ± 1.2	11.5 ± 2.3	12.1 ± 1.4
UTS (MPa)	290.3 ± 1.2	155.6 ± 2.2	59.5 ± 2.5	118.3 ± 4.7	158.8 ± 3.2	196.8 ± 2.6	177.3 ± 3.1
Yield strength (MPa)	288.4 ± 0.9	150.1 ± 1.8	58.3 ± 2.3	109.2 ± 3.1	152.3 ± 2.8	194.03 ± 1.8	174.6 ± 3.2

and grain refinement were subdued by the increased softening effect (i.e., loss of structural strengthening) at 6 weld passes.

Figure 8 reveals the fracture surfaces (SEM images) of the base metal, unreinforced and reinforced weldments after tensile test. Dimples or microvoids formation has been found as indications for ductile fracture, while brittle fracture is often identified by the presence of flat surfaces on the fracture surfaces (Ref 32). The base metal and the unreinforced joint (see Fig. 8a & b) were predominantly characterised by the formation of small dimples. This justifies the high ductility (PE of 21-24%) exhibited by the two samples. The fracture surface of sample C1 (1.72 g SiC, 2 passes), as shown in Fig. 8c, comprises of flat surfaces and some large dimples. This indicates that the sample underwent brittle and ductile fractures. The occurrence of brittle fracture explains the lowest tensile strength and ductility demonstrated by this sample because brittle fracture is often characterised with sudden failure of specimen during tensile test. The occurrence of the brittle fracture can be attributed to high SiC content resulting in particles clustering/agglomeration and low degree of fragmentation.

As the SiC content reduced to 0.56 g (sample A1 in Fig. 8d), the occurrence of the flat surface reduced significantly and more dimples were formed. This was traced to noticeable decrease in particles clustering and increased particles fragmentation. This confirms the improved ductility and strength observed as the SiC content reduced. As the number of weld passes increased (see samples A1, A2 and A3 in Fig 8 d-f), more dimples were formed, smaller dimples emergence increased and the flat surface disappeared. This is an indication that the ductile fracture increasingly occurred and a confirmation for enhanced ductility as the number of weld passes increased. The strength also improved (2-4 passes). This observation is consistent with the findings of *Paidar et al.* (Ref 33).

3.5 Wear Analysis

The variations of volume loss with the sliding distance at 50 N load for some selected samples are presented in Fig. 9a. The volume loss increased with increasing the sliding distance for all samples. The unreinforced joint exhibited the largest amount of material loss ($\sim 4.22 \text{ mm}^3$) at 1000 m sliding distance indicating the highest wear rate since volume loss is proportional to the wear rate. This is due to the loss of structural strengthening which is evident in its significant low hardness ($65 \text{ HV}_{0.3}$) relative to the base metal ($113 \text{ HV}_{0.3}$).

Figure 9b and 8c presents the SWR of some selected at low (20 N) and high load (50 N) conditions. The SWR followed similar trends as the SiC content and number of weld passes increased. However, the wear rate was higher at 50 N load, for all samples, because of increased sliding pressure contact at higher load condition. The unreinforced joint exhibited the highest volume loss hence, highest wear rate under both conditions. Improved wear resistance demonstrated by the reinforced over unreinforced joints is mainly due to two factors. First, the hard particles act as a barrier reducing the pressure contact between the hard disk and soft aluminum matrix. Secondly, the improved grain refinement in the reinforced joint makes the aluminum matrix harder hence, enhanced resistance to wear. As shown in Fig. 9b, the SWR reduced by a factor of 1.83 from $7.71 \times 10^{-5} \text{ mm}^3 \text{ N}^{-1} \text{ m}^{-1}$ to $4.21 \times 10^{-5} \text{ mm}^3 \text{ N}^{-1} \text{ m}^{-1}$ when the SiC content increased from 0.56 g (sample A1) to 1.01 g (Sample B1). Increasing the SiC content to 1.72 g resulted in decline in SWR by a factor of 1.46 to $6.14 \times 10^{-5} \text{ mm}^3 \text{ N}^{-1} \text{ m}^{-1}$. This observation is confirmed by the coefficient of friction (COF) automatically recorded during the wear test. The average COF recorded for samples A1, B1 and C1 is 0.67, 0.54 and 0.66 (see Fig. 10). According to *Mirjavadi et al.* (Ref 34), lower COF implies better wear resistance (i.e., lower wear rate).

The low SiC content in sample A is adjudged to account for its high SWR, compared with the samples B1 and C1. Due to

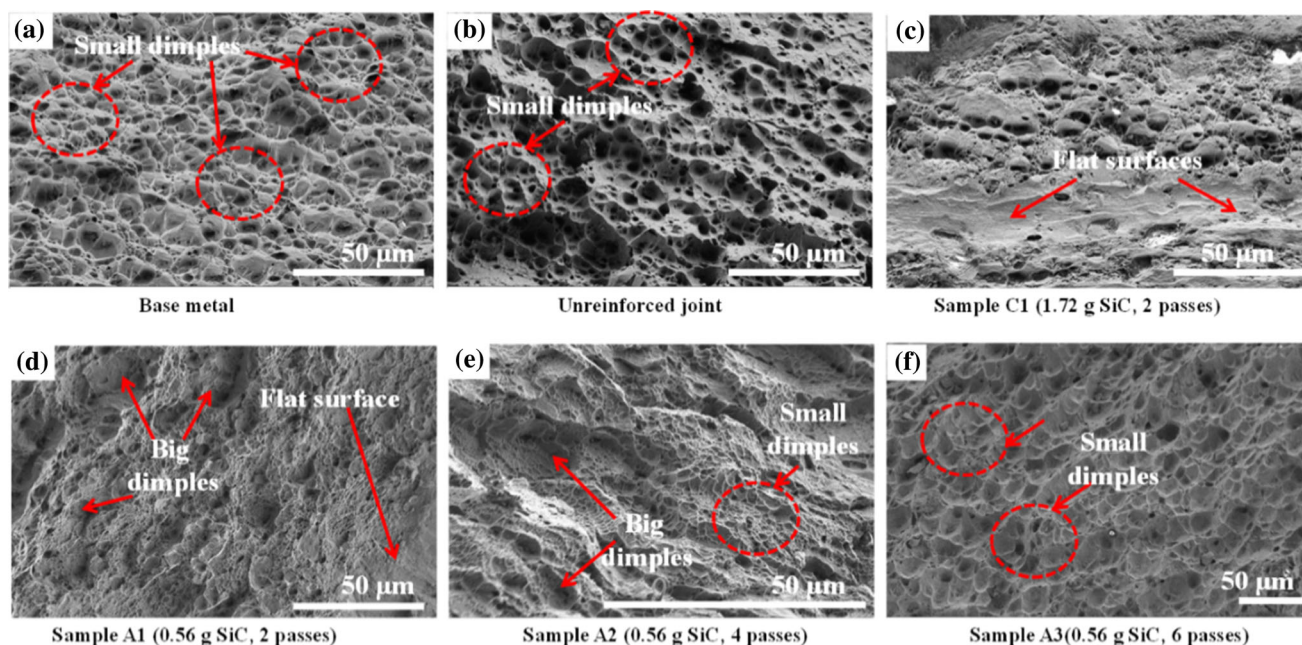


Fig. 8 SEM images revealing the fracture surfaces of the (a) base metal, (b) unreinforced and (c-f) reinforced AA 6061 weldments with varying SiC contents subjected to different passes

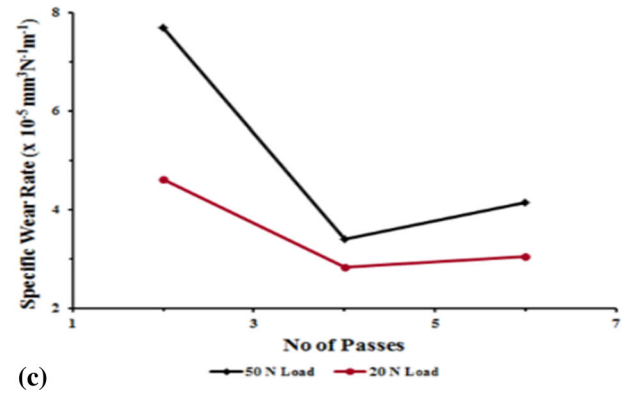
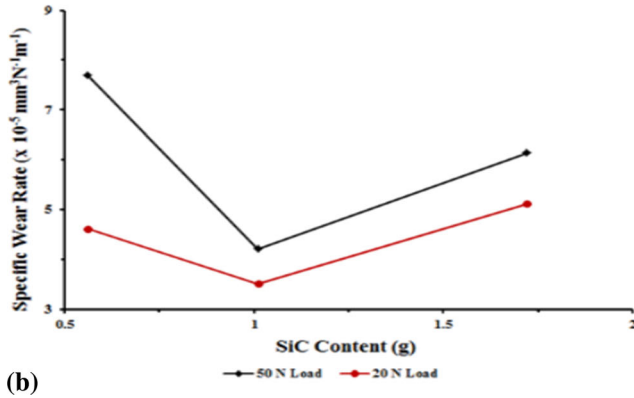
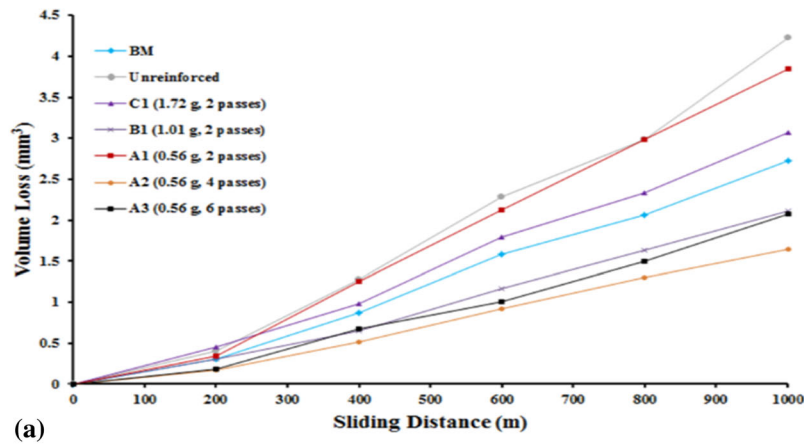


Fig. 9 Wear analysis of SiC reinforced AA 6061-T6 friction stir welded joints showing the plots of (a) volume loss at varying sliding distances (at 50 N Load), (b) specific wear rate against SiC content in the joint and (c) specific wear rate against number of weld passes

this reason, larger surface of the soft aluminum matrix was exposed to the disk contact. Also, the hardness of the joint was found to be the lowest among the three samples (A1, B1, C1). As a result, high volume loss leading to high SWR was found for sample A1. Reduced SWR demonstrated by the sample B1 indicates that the wear resistance improved with the increase in SiC content (from 0.56 to 1.01 g). This is attributed to reduced aluminum matrix volume exposed to the disk contact because more area was occupied by the hard ceramic (SiC) (see Fig. 4). Also, the higher hardness of the joint (compared with the sample A1) contributed to the reduction in the SWR. Despite the highest hardness exhibited by the sample C1 (1.72 g SiC addition), its higher SWR (compared with sample B1) was traced to the clustering of the SiC particles, as evident in Fig. 4. As previously explained in Sect. 3.2, SiC clustering is probably due to hindered tool stirring caused by high volume of SiC addition in the joint. According to *Nosko et al.* (Ref 35), the reinforcement particle-metal matrix cohesion is weaker in the region where there is particle's agglomeration/clustering. As seen in Fig. 11, the large pits seen in the worn surface of the sample C1 are evidence of plowing out of the ceramic particles during the wear test. This shows that abrasive wear mechanism occurred. It is believed that the ceramic particles were easily dislodged because of weaker ceramic particles-aluminum matrix cohesion. This eventually led to serious wear damage (increase volume loss) because more matrix surface was eventually exposed to the hard disk contact.

EDX point and area analyses were conducted on the worn surfaces. The main features analyzed on the worn surfaces in Fig. 12 were spotted as 1, 2, 3 and 4 for alloy and composite, respectively. Table 5 gives the chemical composition of these features. The gray-contrast phase spotted as 1 is highly rich in Fe. The presence of Fe in the entire region of the worn surfaces suggests that initially, asperities of aluminum alloy and steel disk surfaces were meeting each other and eventually welded together by high local pressure forming adhesive bonds. However, during sliding motion, the asperity joints are adjudged to have fractured at the softer aluminum alloy surface (Ref 36). Consequently, material removal from the alloy surface generated wear debris that contains iron. Eventually, the crater (spot 2) has lower iron composition. High oxygen composition found in the crater can be traced to fast oxidation of the fresh metallic surface during exposure to air after the material removal (Ref 37).

Similar explanation is true for composite (SiC-reinforced FSWJ samples) worn surface as there is the evidence of Fe adhesion to composite surface (spot 3) in comparison with pit region (spot 4). However, since hard SiC particles reinforced the aluminum alloy, material loss due to wear is less thus leaving behind more Fe-rich regions on the composite surface compared to those on alloy surface (Fig. 12 c, d). This finding explains the smoother surface found in the composite samples.

As shown in Fig. 9c, the SWR reduced by a factor of 2.3 as the number of weld passes increased from 2 to 4. The SWR at 4 passes (sample A2) is $3.4 \times 10^{-5} \text{ mm}^3 \text{ N}^{-1} \text{ m}^{-1}$ and this is the

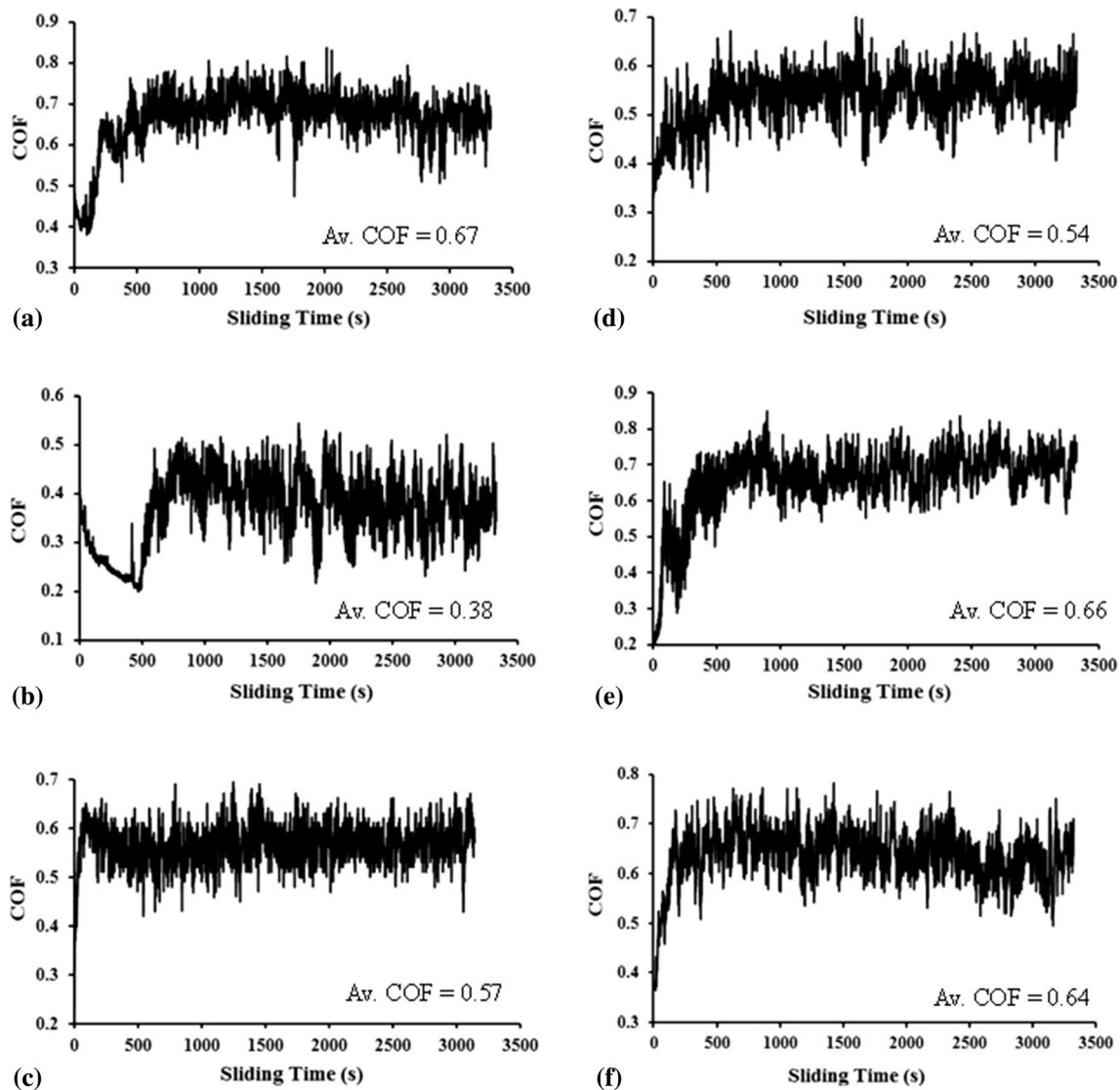


Fig. 10 Coefficient of friction (COF) of the reinforced AA 6061-T6 friction stir welded joints formed with (a) 0.56 g SiC, 2 weld passes (b) 0.56 g SiC, 4 weld passes, (c) 0.56 g SiC, 6 weld passes, (d) 1.01 g SiC, 2 weld passes, (e) 1.72 g SiC, 2 weld passes and (f) the base metal

lowest among the entire samples including the base metal. However, from 4 to 6 weld passes, the wear rate increased by a factor of 1.2. The wear resistance is observed to follow the hardness trend as the number weld passes varied. Also, the average COF recorded (see Fig. 10) for the samples confirmed the trend. Average COF of 0.67, 0.38 and 0.57 was found for the samples A1, A2 and A3, respectively. Besides the higher aluminum matrix hardness, the reduction in the wear rate as the weld passes increased from 2 to 4 is also attributed to enhanced homogeneous SiC dispersion and increased particles fragmentation at 4 passes. Better SiC particles distribution makes the high hardness more uniform throughout the joint. As a result, the disk contact pressure was nearly equally resisted in the entire joint surface. Fragmentation of the particles into smaller sizes aided their uniform distribution, therefore, limiting the disk-aluminum contact in the entire joint surface area.

Also, smaller particles are known to have stronger cohesion with the matrix because larger volume/area of a smaller particle is bonded with the matrix. So, higher number of smaller sized particles found at 4 weld passes contributed to improved wear

resistance. Simply, the drop in the SWR at 6 weld passes can be attributed to further loss of aging effect because of the high welding temperature experienced at 6 weld passes. This resulted in further softening of the matrix leading to increased aluminum matrix removal rate as it contacted the hard disk during the wear test. Hence, the wear resistance of the joint decreased as the weld passes increased from 4 to 6.

3.6 Conclusions

In this work, friction stir welding of SiC-reinforced AA 6061-T6 was successfully performed at optimised process parameters (850 rpm rotational speed, 45 mm min⁻¹ traverse speed and tilt angle of 2.5°) under varying center groove width (1.5-3.5 mm), SiC contents (0.56-1.72 g) and weld passes (2-6). The following findings were obtained;

- (i) A process map predicting the surface characteristics of the SiC-reinforced AA 6061-T6 friction stir welded joints at varying number of weld passes and center groove width (CGW) was successfully developed.

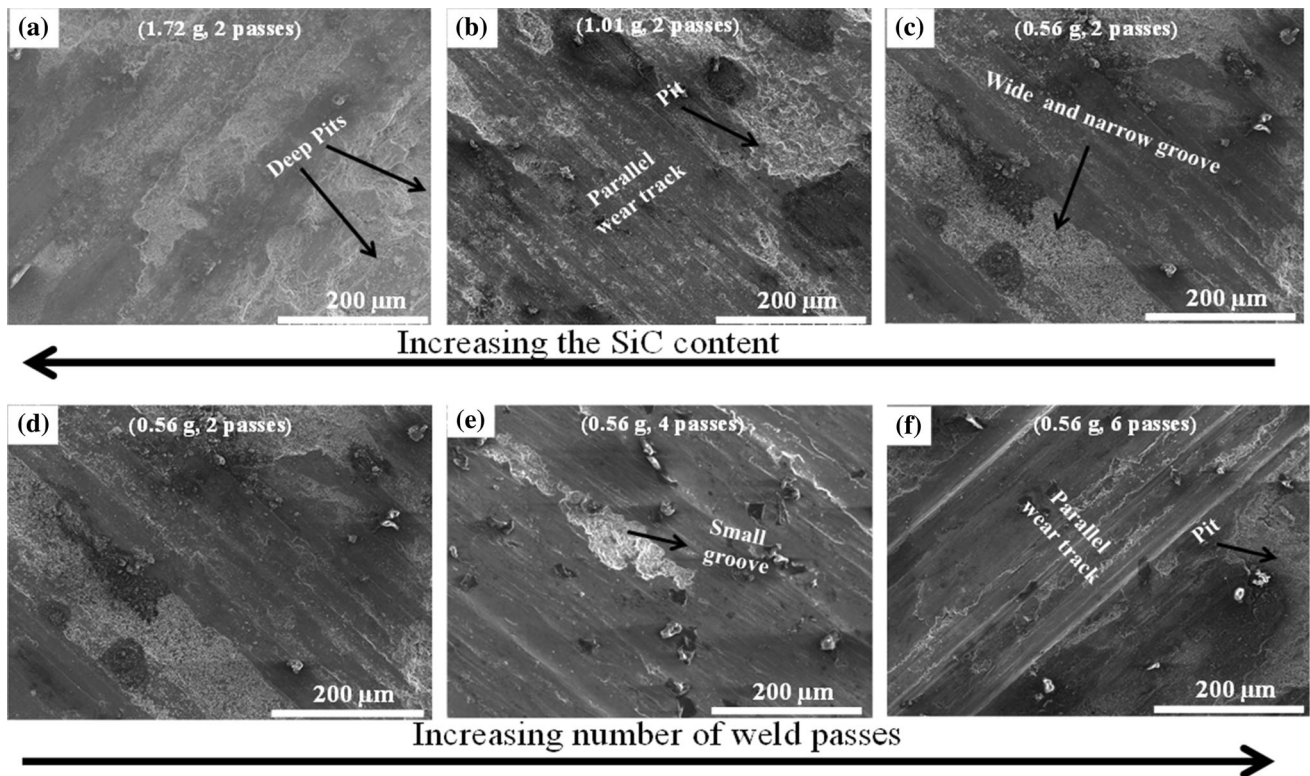


Fig. 11 Worn surfaces of the reinforced AA 6061-T6 friction stir welded joints formed at different SiC contents and varying weld passes

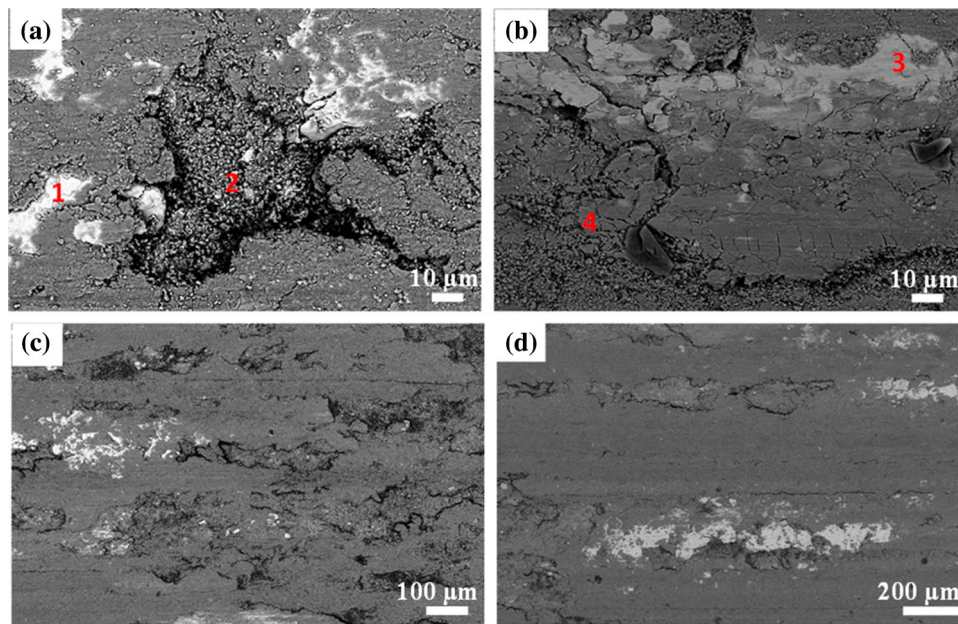


Fig. 12 SEM images showing the regions where EDX analysis was conducted on the worn surfaces

Smooth and strongly bonded joints with no visible surface defect were obtained at CGW of 1.5 mm for 2 to 6 passes and 2.5 mm CGW for only 2 passes.

- (ii) Particles fragmentation and grain refinement increased as the weld passes increased. However, increasing SiC content improved grain refinement but reduced SiC fragmentation. Particles clustering which disappeared as the SiC content reduced and weld passes number increased

was prominent in the joint reinforced with 1.72 g SiC content.

- (iii) All the reinforced joints showed better grain refinement, hardness and wear resistance than the unreinforced joint. Only the joint reinforced with 0.56 g SiC reinforced joint showed higher tensile strength than the unreinforced joint. 0.56 g SiC reinforced joint formed at 4 passes exhibited the best combination of properties with improvement of

Table 5 EDX analysis of the marked spots in Fig.12

Coded regions in Fig.12	Chemical composition wt.%				
	Al	Fe	O	Si	C
1	11.7	52.1	13.2	2.7	20.3
2	44.9	12.6	31.5	0.5	10.5
3	8.6	76.9	5.8	0.8	7.9
4	47.9	23.2	18.8	0.5	9.6

about 26%, 26% and 38% in hardness, tensile strength and wear resistance, respectively, over the unreinforced joint.

- (iv) The hardness increased by 13% as the SiC content increased from 0.56 to 1.72 g. The hardness increased by ~ 8% as the weld passes increased from 2 to 4 passes but at 6 passes, it decreased by ~4% due to predominant aluminum matrix softening effect caused by the excessive dissolution of the strengthening precipitate.
- (v) The tensile strength and percentage elongation decreased with increasing SiC content. The P.E. increased with increasing the weld passes number while the tensile strength also increased until 4 weld passes after which it declined slightly due to the predominant softening effect at 6 weld passes. All the samples experienced ductile fracture except the samples with 1.72 g and 1.01 g of SiC which showed a combination of brittle and ductile fractures.
- (vi) Increase in the weld passes from 2 to 4 reduced the specific wear rate (from $7.71 \times 10^{-5} \text{ mm}^3 \text{ N}^{-1} \text{ m}^{-1}$) by a factor of 2.3 due to better grain refinement and increased particles fragmentation and distribution. However, increased aluminum softening effect at 6 weld passes caused a rise in specific wear rate by a factor of 1.2 to $4.08 \times 10^{-5} \text{ mm}^3 \text{ N}^{-1} \text{ m}^{-1}$. Only the samples formed with 0.56 g SiC content at 4 passes, 1.01 g content at 2 passes and 0.56 g content at 6 passes showed better wear resistance than the base metal.

Acknowledgment

The authors appreciate the funding and support provided by the Universiti Sains Malaysia for Teaching Fellow Scheme and Ministry of Higher Education of Malaysia for FRGS Grant No. 203/PBAHAN/6071386. The technical assistance provided by Mr Sharul and Mr Norshahrizol of the School of Materials and Mineral Resources Engineering, Universiti Sains Malaysia is also appreciated.

References

- V.P. Singh, S.K. Patel, A. Ranjan and B. Kuriachen, Recent research progress in solid state friction-stir welding of aluminium-magnesium alloys: a critical review, *J. Mater. Res. Technol.*, 2020 <https://doi.org/10.1016/j.jmrt.2020.01.008>
- M. Marini and A.B. Ismail, Torsional deformation and fatigue behaviour of 6061 aluminium alloy, *IJUM Eng. J.*, 2011, **12**, p 21–32
- S. Rajakumar, C. Muralidharan and V. Balasubramanian, Establishing empirical relationships to predict grain size and tensile strength of

- friction stir welded AA 6061–T6 aluminium alloy joints, *Trans. Nonferrous Metals Soc. China*, 2010, **20**, p 1863–1872
- T.E. Abioye, N. Mustar, H. Zuhailawati and I. Suhaina, Prediction of the tensile strength of aluminium alloy 5052–H32 fibre laser weldments using regression analysis, *Int. J. Adv. Manuf. Technol.*, 2019, **102**, p 1951–1962
- O.S. Salih, H. Ou, W. Sun and D.G. McCartney, A review of friction stir welding of aluminium matrix composites, *Mater. Des.*, 2015, **86**, p 61–71
- M. Reimann, T. Gartner, U. Suhuddin, J. Göbel and J.F. dos Santos, Keyhole closure using friction spot welding in aluminum alloy 6061–T6, *J. Mater. Process. Technol.*, 2016, **237**, p 12–18
- W. Safeen, S. Hussain, A. Wasim, M. Jahanzaib, H. Aziz and H. Abdalla, Predicting the tensile strength, impact toughness and hardness of friction stir-welded AA6061-T6 using response surface methodology, *Int. J. Adv. Manuf. Technol.*, 2016, **87**, p 1765–1781
- M.F. Nikoo, H. Azizi, N. Parvin and H.Y. Naghibi, The influence of heat treatment on microstructure and wear properties of friction stir welded AA6061-T6/Al₂O₃ nanocomposite joint at four different traveling speed, *J. Manuf. Process.*, 2016, **22**, p 90–98
- C.M.A. Fernandez, R.A. Rey, M.J.C. Ortega, D. Verdura and C.L. Vidal, Friction stir processing strategies to develop a surface composite layer on AA6061-T6, *Mater. Manuf. Processes*, 2018, **33**, p 1133–1140
- T. Singh, S.K. Tiwari and D.K. Shukla, Friction stir welding of AA6061-T6: The effect of Al₂O₃ nanoparticles addition, *Results Mater.*, 2019, **1**, p 1–12
- N. Gangil, A.N. Siddiquee and S. Maheshwari, Aluminium based in-situ composite fabrication through friction stir processing: a review, *J. Alloy. Compd.*, 2017, **715**, p 91–104
- H. Kumar, R. Prasad, A. Srivastava, M. Vashista and M.Z. Khan, Utilization of industrial waste (Fly ash) in the synthesis of copper-based surface composite through friction stir processing route for wear applications, *J. Clean. Prod.*, 2018, **196**, p 460–468
- K.O. Babaremu and O.O. Joseph, Experimental study of corncob and cow horn AA6063 reinforced composite for improved electrical conductivity, *J. Phys.: Conf. Ser.*, 2019, **1378**, p 1–8
- R. Maurya, B. Kumar, S. Ariharan, J. Ramkumar and K. Balani, Effect of carbonaceous reinforcements on the mechanical and tribological properties of friction stir processed Al6061 alloy, *Mater. Des.*, 2016, **98**, p 155–166
- S. Selvakumar, I. Dinaharan, R. Palanivel and B. Ganesh Babu, Development of stainless steel particulate reinforced AA6082 aluminium matrix composites with enhanced ductility using friction stir processing, *Mater. Sci. Eng.: A*, 2017, **685**, p 317–326
- V.K. Mohan, M. Shannadh and A. Sudheer, Fabrication and characterization of friction stir welding of AA6061 using copper powder, *Mater. Today: Proc.*, 2018, **5**, p 24339–24346
- V.M. Khojastehzhad and H.H. Poursal, Microstructural characterization and mechanical properties of aluminum 6061–T6 plates welded with copper insert plate (Al/Cu/Al) using friction stir welding, *Trans. Nonferrous Metals Soc. China*, 2018, **28**, p 415–426
- D.-H. Choi, Y.-I. Kim, D.-U. Kim and S.-B. Jung, Effect of SiC particles on microstructure and mechanical property of friction stir processed AA6061-T4, *Trans. Nonferrous Metals Soc. China*, 2012, **22**, p 614–618
- P. Asadi, M.K. Besharati Givi, K. Abrinia, M. Taherishargh and R. Salekrostam, Effects of SiC particle size and process parameters on the microstructure and hardness of AZ91/SiC composite layer fabricated by FSP, *J. Mater. Eng. Perform.*, 2011, **20**, p 1554–1562
- T.E. Abioye, H. Zuhailawati, A.S. Anasyida, S.A. Yahaya and B.K. Dhindaw, Investigation of the microstructure, mechanical and wear properties of AA6061-T6 friction stir weldments with different particulate reinforcements addition, *J. Market. Res.*, 2019, **8**, p 3917–3928
- S. Sahraeinejad, H. Izadi, M. Haghshenas and A.P. Gerlich, Fabrication of metal matrix composites by friction stir processing with different particles and processing parameters, *Mater. Sci. Eng.: A*, 2015, **626**, p 505–513
- T. Prater, B. Gibson, C. Cox, G.E. Cook and A.M. Strauss, Effect of particle size on tool wear in friction stir welding of al 6061 with silicon carbide reinforcement, *J. Manuf. Technol. Res.*, 2014, **6**, p 125–142
- P.N. Karakizis, D.I. Pantelis, G. Fourlaris and P. Tsakiridis, Effect of SiC and TiC nanoparticle reinforcement on the microstructure, micro-

- hardness and tensile performance of AA6082-T6 friction stir welds, *Int. J. Adv. Manuf. Technol.*, 2018, **95**, p 3823–3837
24. M. Rahsepar and H. Jarahimoghadam, The influence of multi-pass friction stir processing on the corrosion behaviour and mechanical properties zircon-reinforced Al metal matrix composites, *Mater. Sci. Eng.: A*, 2016, **671**, p 214–220
 25. R.R. Baridula, A.B. Ibrahim, C.K.M. Faizal, B.C.K. Yahya, R. Kulkarni, R.V. Ramaraju, (2018) Influence of groove size and reinforcements addition on mechanical properties and microstructure of friction stir welded joints, *IOP Conf. Series: Materials Science and Engineering*, **319**, p 1-8
 26. M.N. Ahmad Fauzi, M.B. Uday, H. Zuhailawati and A.B. Ismail, Microstructure and mechanical properties of alumina-6061 aluminum alloy joined by friction welding, *Mater. Design*, 2010, **31**, p 670–676
 27. M. Bodaghi and K. Dehghani, Friction stir welding of AA5052: the effects of SiC nano-particles addition, *Int. J. Adv. Manuf. Technol.*, 2017, **88**, p 2651–2660
 28. B. Sattari, M. Shamanian, A. Ashrafi, M. Salehi and F. Salimijazi, Effect of number of passes on the corrosion behaviour of Fe/Al surface composites produced by plasma spraying and friction stir processing, *J. Mater. Process. Technol.*, 2017, **250**, p 35–44
 29. H.M. Jamalain, H. Ramezani, H. Ghobadi, M. Ansari, S. Yari and M.K.B. Givi, Processing-structure-property correlation in nano-SiC-reinforced friction stir welded aluminium joints, *J. Manuf. Process.*, 2016, **21**, p 180–189
 30. A. Kar, S. Suwas and S.V. Kailas, Two-pass friction stir welding of aluminium alloy to titanium alloy: a simultaneous improvement in mechanical properties, *Mater. Sci. Eng.: A*, 2018, **733**, p 199–210
 31. P. Periyasamy, B. Mohan and V. Balasubramanian, Effect of Heat Input on Mechanical and Metallurgical Properties of Friction Stir Welded AA6061-10% SiCp MMCs, *J. Mater. Eng. Perform.*, 2012, **21**, p 2417–2428
 32. R. Bobbili, V. Madhu and A.K. Gogia, Tensile behaviour of aluminium 7017 alloy at various temperatures and strain rates, *J. Market. Res.*, 2016, **5**, p 190–197
 33. M. Paidar, O.O. Ojo, H.R. Ezatpour and A. Heidarzadeh, Influence of multi-pass FSP on the microstructure, mechanical properties and tribological characterization of Al/B4C composite fabricated by accumulative roll bonding (ARB), *Surf. Coat. Technol.*, 2019, **361**, p 159–169
 34. S.S. Mirjavadi, M. Alipour, S. Emami, S. Kord, A.M.S. Hamouda, P.G. Koppad and R. Keshavamurthy, Influence of TiO₂ nanoparticles incorporation to friction stir welded 5083 aluminum alloy on the microstructure, mechanical properties and wear resistance, *J. Alloy. Compd.*, 2017, **712**, p 795–803
 35. M. Nosko, M. Štěpánek, P. Zifčák, L. Orovčík, Š. Nagy, T. Dvorák, P. Oslanec, F. Khodabakhshi and A.P. Gerlich, Solid-state joining of powder metallurgy Al-Al₂O₃ nanocomposites via friction-stir welding: effects of powder particle size on the weldability, microstructure, and mechanical property, *Mater. Sci. Eng.: A*, 2019, **754**, p 190–204
 36. B.T. Ogunsemi, T.E. Abioye, T.I. Ogedengbe and H. Zuhailawati, A review of various improvement strategies for joint quality of AA 6061–T6 friction stir weldments, *J. Mater. Res. Technol.*, 2021, **11**, p 1061–1089
 37. A. Moharrami, A. Razaghian, M. Paidar, M. Slapakova, O.O. Ojo and R. Taghiabadi, Enhancing the mechanical and tribological properties of Mg₂Si-rich aluminum alloys by multi-pass friction stir processing, *Mater. Chem. Phys.*, 2020, **250**, p 123066

Publisher's Note Springer Nature remains neutral with regard to jurisdictional claims in published maps and institutional affiliations.